The High Frequency Effects on Multilayer Graphene Ribbon Based THz Resonators

Haotian Zhang, Min Tang, and Jun-Fa Mao
Key Laboratory of Ministry of Education of Design and Electromagnetic Compatibility of High-Speed Electronic Systems, Shanghai Jiao Tong University, Shanghai, China 200240
Email: fn2878@sjtu.edu.cn, tm222@sjtu.edu.cn, jfmao@sjtu.edu.cn

***Abstract* — Graphene has been proved to be one of the promising candidate materials for high-frequency applications. The multilayer graphene ribbon (GR) based resonators are proposed and characterized in this work. The geometry-dependent resonant frequencies (f_0) and unloaded Q-factors (Q_u) of the GR-based resonators are investigated with the equivalent single conductor (ESC) model. It is found that by intercalation doping with AsF_5, the graphene resonators can provide a high Q_u of 80.6 at f_0=793.1 GHz, superior to the copper and neutral graphene based ones.**

***Index Terms* — Equivalent single conductor (ESC) model, graphene ribbon (GR), intercalation doping, resonator.**

I. Introduction

The excellent mechanical, thermal and electrical properties of carbon nanomaterials make them very attractive for various applications [1], [2]. Based on the unique electrical properties of carbon nanotubes (CNT), a multiwalled CNT based resonator is proposed and analyzed using the methods of multiconductor transmission line (MTL) and equivalent single conductor (ESC) [3]. It is shown that this kind of resonator can outperform the copper counterpart, especially in low THz frequency range. On the other hand, graphene shares most of the outstanding properties of CNT and has even better process controllability due to its planar structure. Besides, the electrical conductivity of graphene can be dramatically improved by proper intercalation doping [4], which implies promising applications of high-performance passive devices at microwave and low THz frequencies.

In this paper, a graphene ribbon (GR) based half-wavelength resonator is proposed. Its good performance is quantitatively investigated and compared with the copper counterpart. Three kinds of graphene recipes, including neutral graphene, stage-1 and stage-2 AsF_5 intercalated graphenes, are considered here. The equivalent circuit model is established for ESC method by using the extracted parameters of GRs. Resonant frequencies and Q-factors are then predicted for the graphene resonators.

II. Modelling and Analysis

Fig. 1 shows the configuration of the proposed graphene resonator, which is an open-ended multilayer GR placed on a SiO_2 substrate with a thickness of H. The width, length and thickness of GR are denoted by w, l and t, respectively. Two metal (Au) pads are assigned at the two ends.

The performance of resonator is mainly determined by the physical properties of graphene and the geometry. The typical parameters are listed in Table I for three recipes, i.e. the neutral graphene, the stage-1 and stage-2 AsF_5 graphite intercalation compounds [1], [5], where σ_{DC} is the in-plane conductivity, n_p is the hole volume concentration, and S is the average spacing between two adjacent graphene layers. The Fermi level E_F of GR can be extracted using the hole density per layer n_{p0} by

$$E_F = \hbar v_F \sqrt{\pi n_{p0}} = \hbar v_F \sqrt{\pi n_p S}\ . \qquad (1)$$

where $\hbar$ is the reduced Plank's constant, v_F=10^6 m/s is the Fermi velocity. For low THz frequencies, the intraband contribution dominates the surface conductivity of graphene, given by [6]

$$\sigma = \frac{\sigma_{DC}}{1+j\omega\tau} = \frac{e^2 K_B T \tau}{\pi\hbar^2 (1+j\omega\tau)}\left[\frac{E_F}{K_B T} + 2\ln\left(e^{-\frac{E_F}{K_B T}}+1\right)\right], \qquad (2)$$

$$l_D = 2 v_F \tau\ . \qquad (3)$$

where e is the elementary charge, K_B is Boltzmann's constant, τ is the momentum relaxation time, and T is the temperature. The value of τ can be extracted from the DC conductivity by (2), and then the mean free path (MFP) l_D of carriers in graphene is obtained by (3) [1].

TABLE I
Parameters of Three Graphene Recipes

Graphene recipes	σ_{DC} $(\mu\Omega\cdot\mathrm{cm})^{-1}$	n_p (cm^{-3})	S (nm)	E_F (eV)	τ (ps)	l_D (μm)
Neutral	0.026	-	0.34	0	0.21	0.42
Stage-1 AsF_5	0.49	3.2×10^{20}	0.815	-0.60	0.57	1.14
Stage-2 AsF_5	0.63	4.6×10^{20}	0.575	-0.60	0.52	1.03

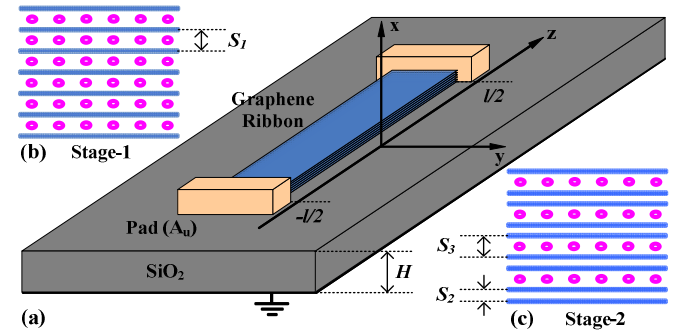

Fig. 1. Schematic views of: (a) the proposed GR resonator; (b) the stage-1 and (c) the stage-2 AsF_5 intercalation doped GRs.

The per unit length (*p.u.l*) impedance, scattering resistance and kinetic inductance are given by

$$Z_{SLG} = \frac{1}{\sigma w} = \frac{1}{\sigma_{DC} w} + j\omega\frac{\tau}{\sigma_{DC} w} = R_s + j\omega L_k . \quad (4)$$

The quantum resistance for each layer is $R_q=R_s l_D$. The quantum capacitance of GR is calculated by [7]

$$C_q = \frac{2e^2 K_B T}{\pi(\hbar v_F)^2}\ln\left[2\left(1+\cosh\frac{E_F}{K_B T}\right)\right]. \quad (5)$$

The *p.u.l* mutual inductance and electrostatic capacitance between adjacent layers are given by

$$C_E = \varepsilon_0\varepsilon_r w/S,\ L_M = \mu_0 S/w . \quad (6)$$

where ε_r=5.1 is the relative permittivity of AsF_5. The tunneling effect between adjacent layers can be characterized by the *c*-axis conductivity in [5]. Since this conductivity is much smaller than the in-plane conductivity, the tunneling conductance is neglected in our modeling. The electrostatic capacitance and magnetic inductance between the bottommost layer of GR and ground plane are approximated as a microstrip structure by

$$C_{E,N} = \sqrt{\varepsilon_{re}\varepsilon_0\mu_0}/Z_c,\ L_{M,N} = Z_c\sqrt{\varepsilon_{re}\varepsilon_0\mu_0}, \quad (7)$$

$$Z_c = \frac{60}{\sqrt{\varepsilon_{re}}}\ln\left(\frac{8H}{w}+\frac{w}{4H}\right), \quad (8)$$

$$\varepsilon_{re} = \frac{\varepsilon_{SiO2}+1}{2}+\frac{\varepsilon_{SiO2}-1}{2}\left[\left(1+12\frac{H}{w}\right)^{-0.5}+0.041\left(1-\frac{w}{H}\right)^2\right]. \quad (9)$$

where ε_{SiO2}=3.9 is the relative permittivity of SiO_2 substrate.

As shown in Fig. 2, the equivalent *p.u.l* resistance, inductance and capacitance are obtained according to the ESC method [8], which is based on the assumption that arbitrary cross section of the multilayer GR is equipotential. Then, the GR can be regarded as a single transmission line, whose characteristic impedance and propagation constant are calculated by

$$Z_0 = \sqrt{(R_{ESC}+j\omega L_{ESC})/j\omega C_{ESC}}, \quad (10)$$

$$\gamma = \sqrt{j\omega C_{ESC}(R_{ESC}+j\omega L_{ESC})}. \quad (11)$$

The perfect contact is assumed in our work, and then the equivalent resistance of each contact between the GR and metal pad is just a half of the quantum resistance R_q. The pad capacitance C_{pad} at the two ends of the resonator is extracted with ANSYS Q3D.

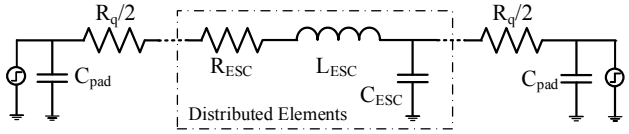

Fig. 2. ESC circuit model of the GR resonator.

For the odd mode of the half-wavelength resonator, the input admittance of half circuit, looked from one open end, is

$$Y_{in,ESC} = j\omega C_{pad} + \left[Z_0\tanh(\gamma l/2)+R_q/2\right]^{-1}. \quad (12)$$

Then, we have $\mathrm{Im}(Y_{in,ESC})$=0 at the dominant odd-mode resonant frequency ω_0.

Considering different power dissipation in the GR-based resonator, the unloaded *Q*-factor Q_u is calculated by [3]

$$1/Q_u = 1/Q_{GR}+1/Q_c+1/Q_{GND}+1/Q_r . \quad (13)$$

where Q_{GR} corresponds to the loss in GR, Q_c describes the power loss due to the contact resistance between the GR and metal pads, Q_{GND} is according to the loss in the ground plane, and Q_r is the *Q*-factor due to the radiation loss.

III. Results and Discussion

Based on the above modeling method, the resonant frequency and *Q*-factors of the proposed GR-based resonator are analyzed. The typical geometric parameters are *l*=100 μm, *w*=4 μm, *t*=0.5 μm and *H*=10 μm.

The variation of resonant frequency and unloaded *Q*-factor with different ribbon width is plotted in Fig. 3. The characteristics of the resonators based on three graphene recipes are compared with those of the conventional copper resonator of the same geometry. It should be noted that the size effect must be considered when evaluating copper conductivity due to the small cross section and high operating frequencies [9]. It is seen that the resonant frequency of copper resonator is higher than those of the graphene ones. As to the unloaded *Q*-factor, the neutral GR resonator provides a poor result, even worse than the copper counterpart. However, intercalation doping with AsF_5 can significantly improve the dissipation performance. Both the stage-1 and stage-2 GR resonators possess higher Q_u than the copper one. The stage-2 GR-based resonator shows the best performance, due to the largest volume conductivity.

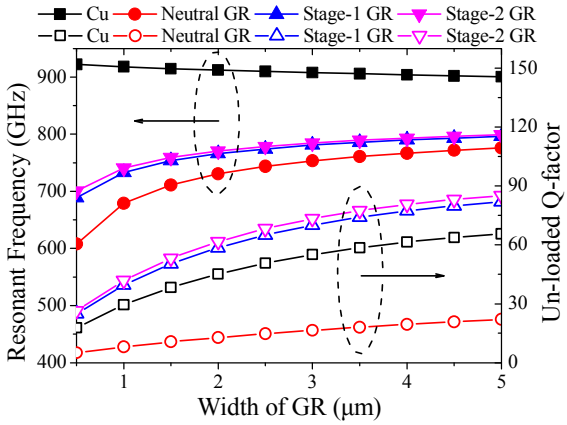

Fig. 3. Resonant frequencies and unloaded *Q*-factors of the GR-based and copper resonators, with *l*=100 μm, *t*=0.5 μm, *H*=10 μm and different width *w*.

Both R_s and L_k are inversely proportional to the GR width *w*. Thus, wider GRs lead to higher resonant frequency, as shown in Fig. 3. However, the decreasing of equivalent magnetic inductance with the increasing of *w* is slower than the variation trend of kinetic inductance. So the GR-based resonator with larger width provides higher value of Q_{GR}, as shown in Fig. 4. It is also noted that Q_{GR} dominates the value of Q_u. Therefore, a wider GR-based resonator provides better unloaded *Q*-factor of Q_u.

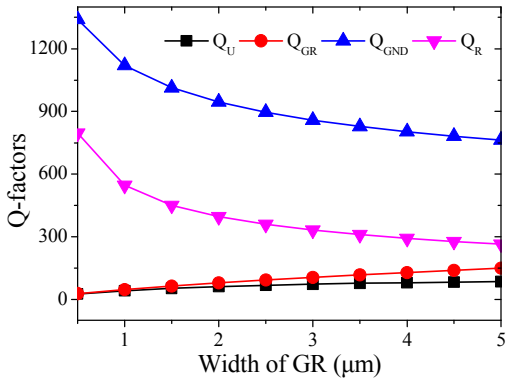

Fig. 4. Q-factors of stage-2 GR resonator due to the losses of GR, ground, radiation and all losses, with l=100 μm, t=0.5 μm, H=10 μm and different width w.

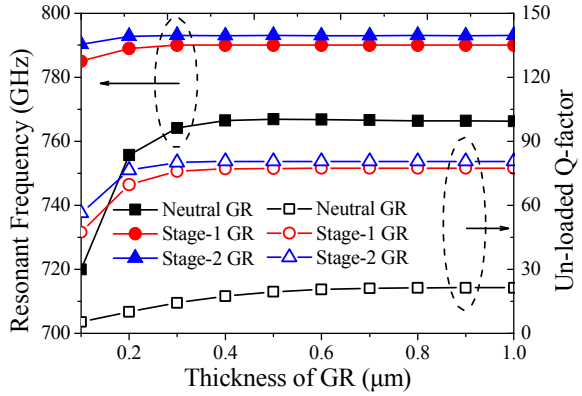

Fig. 5. Resonant frequencies and unloaded Q-factors of the GR-based resonator with w=4 μm, l=100 μm, H=10 μm and different GR thickness t.

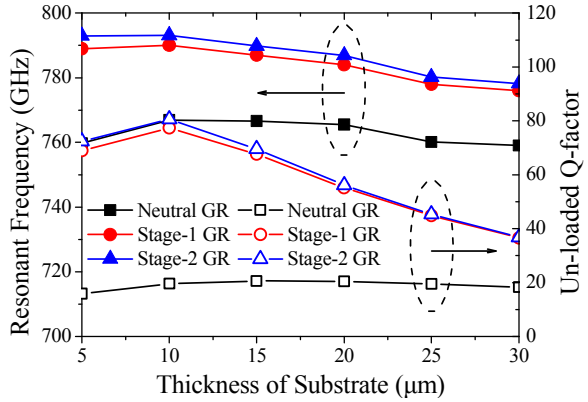

Fig. 6. Resonant frequencies and unloaded Q-factors of the GR-based resonator with w=4 μm, l=100μm, t=0.5 μm and different thickness H of SiO_2 substrate.

Fig. 5 shows the characteristics of GR-based resonators when varying the thickness t of GRs. It is seen that both the resonant frequencies and unloaded Q-factors increase with the GR thickness when t is below 0.5 μm. For thicker GRs, the resonator performance will saturate.

Fig. 6 shows the impact of the substrate thickness on the GR-based resonators. The resonant frequencies with the three graphene recipes all change slightly with the variation of H. For thin substrates, the unloaded Q-factors are dominated by Q_{GR}, leading to the increasing of Q_u with H. For thick substrates, the radiation loss increases rapidly with H and tends to dominate the overall power dissipation. Then, the values of Q_u are reduced in these cases. Therefore, by properly selecting the substrate thickness, an optimal unloaded Q-factor can be achieved. The stage-2 AsF_5 intercalation doped GR resonator is able to provide a high Q_u of 80.6 at f_0=793.1 GHz, when deposited on a 10-μm-thick SiO_2 substrate.

IV. Conclusion

In this paper, new resonators are proposed using multilayer GRs with three different recipes for low THz applications. Their characteristics are investigated by using the ESC model. The impacts of some critical geometric parameters, including the width and thickness of GRs and the substrate thickness, on the resonant frequencies and unloaded Q-factors are also explored numerically. Simulated results indicate the better performance of intercalation doped GR-based resonators than the copper and neutral GR-based counterparts. It is expected that intercalation doped graphenes can be applied in high-performance passive devices within low THz frequency range.

Acknowledgement

This work is supported by the National Natural Science Foundation of China under Grant 61331004.

References

[1] C. Xu, H. Li, and K. Banerjee, "Modeling, analysis, and design of graphene nano-ribbon interconnects," *IEEE Trans. Electron Devices*, vol. 56, no. 8, pp. 1567-1578, Aug. 2009.

[2] D. Sarkar, C. Xu, H. Li, and K. Banerjee, "High-frequency behavior of graphene-based interconnects-part II: impedance analysis and implications for inductor design," *IEEE Trans. Electron Devices*, vol. 58, no. 3, pp. 853-859, Mar. 2011.

[3] Y. Huang, L.-S. Wu, M. Tang, and J.-F. Mao, "High-performance resonator based on multiwalled carbon nanotube (MWCNT)," *IEEE Trans. Nanotechnology*, vol. 13, no. 6, pp. 1240-1249, Nov. 2014.

[4] I. Khrapach, F. Withers, T. H. Bointon, D. K. Polyushkin, W. L. Barnes, S. Russo, and M. F. Craciun, "Novel highly conductive and transparent graphene based conductors," *Advanced Materials*, vol. 24, no. 21, pp. 2844-2849, Apr. 2012.

[5] M. S. Dresselhaus and G. Dresselhaus, "Intercalation compounds of graphite," *Advances in Physics*, vol. 30, no. 2, pp. 139-326, Mar. 1981.

[6] G. W. Hanson, "Quasi-transverse electromagnetic modes supported by a graphene parallel-plate waveguide," *Journal of Applied Physics*, vol. 104, no. 8, pp. 084314-1-5, Oct. 2008.

[7] T. Fang, A. Konar, H. Xiang, and D. Jena, "Carrier statistics and quantum capacitance of graphene sheets and ribbons," *Appl. Phys. Lett.*, vol. 91, no. 9, pp. 092109-1-3, Aug. 2007.

[8] M. S. Sarto, and A. Tamburrano, "Single-conductor transmission -line model of multiwall carbon nanotubes," *IEEE Trans. Nanotechnology*, vol. 9, no. 1, pp. 82-92, Jan. 2010.

[9] H. Li, and K. Banerjee, "High-frequency analysis of carbon nanotube interconnects and implications for on-chip inductor design," *IEEE Trans. Electron Devices*, vol. 56, no. 10, pp. 2202-2214, Oct. 2009.